UC Merced
UC Merced Previously Published Works

Title

One-Step Ligand-Exchange Method to Produce Quantum Dot—DNA Conjugates for DNA-Directed Self-Assembly

Permalink

https://escholarship.org/uc/item/1zb3z0s2

Journal

ACS Applied Materials & Interfaces, 14(42)

ISSN

1944-8244

Authors

Rahmani, Paniz
Goodlad, Melissa
Zhang, Yehan
et al.

Publication Date

2022-10-26

DOI

10.1021/acsami.2c10580

Copyright Information

Peer reviewed

One-Step Ligand Exchange Method to Produce Quantum Dot - DNA Conjugates for DNA Directed Self-Assembly

Paniz Rahmani,[l] Melissa Goodlad,[l] Yehan Zhang,[l] Yichen Li,[†] and Tao Ye[l,†,*]

[l]Department of Chemistry & Biochemistry and [†]Department of Materials and Biomaterials Science & Engineering, 5200 N. Lake Rd, University of California, Merced, California 95343, U. S. A.

ABSTRACT: To address the current challenges in making bright, stable, and small DNA-functionalized quantum dots, we have developed a one-step ligand exchange method to produce QD-DNA conjugates from commonly available hydrophobic quantum dots. We show that by systematically adjusting the reaction conditions such as ligand to nanoparticle ratio, pH, and solvent composition, stable and highly photoluminescent water-soluble DNA-QD conjugates with relatively high ligand loadings can be produced. Moreover, by site-specifically binding these QD-DNA conjugates to a DNA origami template, we demonstrate that these bioconjugates have sufficient colloidal stability for DNA-directed self-assembly. Fluorescence quenching by an adjacent gold nanoparticle (AuNP) was demonstrated. Such QD-AuNP dimers may serve as biosensors with improved sensitivity and reproducibility. Moreover, our simple method can facilitate the assembly of QDs into more complex superlattices and discrete clusters that may enable novel photophysical properties.

INTRODUCTION:

Assemblies of colloidal quantum dots (QDs) may allow individual QDs to couple to enable novel collective properties, such as super-radiance,[1] energy transfer[2] and have potential applications in data storage,[3] energy harvesting,[4] to information processing.[5,6]Among numerous nanoparticle self-assembly methods, DNA mediated self-assembly received considerable attention due to its ability to produce some of the most complex structures including 1D, 2D, and 3D superlattices as well as geometrically complex clusters.[5, 7, 8] To allow the information encoded in the DNA sequence to direct the self-assembly of QDs, these nanoparticles must be conjugated with DNA ligands.[9] QD - DNA conjugates are also bright, photostable, wavelength-tunable emitters that are appealing for sensing and bioimaging.[10-12]

While such conjugates may be produced from hydrophilic QDs that are directly synthesized in the aqueous phase, they are more often produced from hydrophobic-ligands-capped QDs that are synthesized through an organometallic route,[13-16] which ensures a narrow size distribution and high photoluminescence quantum yields. However, the conversion of such hydrophobic QDs into ones that are highly stable in aqueous buffers and have the smallest possible sizes remains challenging. To make the QDs soluble in water, many conjugation methods first encapsulate the hydrophobic QDs with a bifunctional coating, such as silica, amphiphilic polymers, or phospholipids containing aliphatic chains and polar head groups, and then link DNA to the coating.[17-19] While such coatings improve the stability of QDs in aqueous solutions, the increase in the shell thickness weakens the coupling between QDs and makes them undesirable for enabling emergent functions such as

energy transfer,[20-22] the hydrophobic ligands can be first replaced with small amphiphilic ligands that render the QDs water-soluble.[23, 24] Dispersed in an aqueous solution, these QDs can then be conjugated with oligonucleotides through bioconjugation reactions such as amide coupling,[25-28] ligand exchange[29] or peptide-PNA conjugation.[30] While the coupling reactions and two-step cap exchange strategy produce QDs with smaller hydrodynamic sizes, the steric hindrance at the surface of the particles and low colloidal stability often limit the coupling efficiencies, making this method less suitable for many applications that require dense packing of DNA ligands, such as DNA mediated self-assembly of superlattices[31] and DNA origami mediated self-assembly of clusters.[32-35]

Lastly, QD-DNA conjugates can be produced by embedding the end part of the DNA ligands in a passivating shell.[34, 36, 37] While these QD-DNA conjugates have small sizes as well as excellent chemical and photophysical stability, wider adoption of this method is hindered by the requisite expertise in QD synthesis, broadened size distribution and PL band, as well as reduced crystallinity.[38] Due to the difficulties in forming QD-DNA conjugates that are compact, stable, and have the smallest possible size, the reported successes in DNA mediated self-assembly of QDs are notably more limited compared to those in DNA mediated self-assembly of gold nanoparticles,[39-42] which are more readily conjugated with DNA ligands,[43-47] into a large variety of well as discrete clusters.[31, 40]

Here we report a one-pot ligand exchange/phase transfer process that uses hydrophobic QDs to produce QD-DNA conjugates that are compact, bright, and stable in aqueous solutions. We found that our ligand exchange process can directly replace the hydrophobic ligands on commercially available QDs with thiol-modified DNA and transfer the QDs

into an aqueous phase. These DNA conjugated QDs are as emissive as their hydrophobic counterparts. We demonstrate that these QD-DNA conjugates, possessing high colloidal stability, can site-specifically bind to DNA origami templates. Fluorescence quenching by an adjacent gold nanoparticle was demonstrated. Our simple method, which can be readily carried out without expertise in QD synthesis, can facilitate the assembly of QDs into more complex superlattices and discrete clusters that may enable novel photophysical properties.

EXPERIMENTAL SECTION

DNA preparation

The disulfide bonds of 18-nt (5' CA TGT TCA GCG TAA TTTT/(CH2)3SH 3') modified oligonucleotide (from IDT DNA) were cleaved by mixing 100 μM of oligonucleotides with 100 mM tris(2-carboxyethyl) phosphine (TCEP) in a 1:600 ratio and left at room temperature overnight. The TCEP-reduced 18-nt DNA was purified with 3K Da Amicon Ultra-0.5 Centrifugal Filter (Millipore Sigma, Burlington, MA, USA) twice at $14000 \times g$ for 20 minutes and the concentration was measured with Thermo Scientific Nanodrop spectrophotometer. Then the solution mixture was replenished with 1 μl of 100 mM TCEP. it is known that TCEP helps to retain the photoluminescence by suppressing surface etching of the quantum dots. Then the mixture was diluted with Millipore water to minimize the chance of aggregation.

Phase transfer/ligand exchange

Octadecylamine capped CdSe/ZnS QDs in a solid form (Sigma Aldrich, Product #: 748080) were first dissolved in chloroform. The concentration was then measured using the extinction coefficient and absorbance. Previously reduced and purified 18-nt DNA (5' CA TGT TCA GCG TAA TTTT/(CH2)3SH 3') was used for surface functionalization. To find the optimal condition for this reaction, Reaction mixtures with DNA/QD ratios of 20, 80, 160, 320, 640 were prepared with the following condition: reduced DNA-TCEP mixture, 50 μl of dimethyl sulfoxide (DMSO), and 100 μl of chloroform was added to each vial, followed by the addition of the QDs (typically 2.44 μM). Due to slow evaporation during the reaction, chloroform was replenished during the phase transfer. A previous study[48] has shown that zinc ions in the solution help to preserve the QD photoluminescence by passivating the electron surface/hole traps.[20, 22] Therefore, 9 μl of 25 mM $Zn(NO_3)_2$ was added to the reaction to retain the photoluminescence. The mixtures were left on the vortex for at least 0.5 hr. before the addition of NaOH. This stepwise addition of NaOH is typically done at 1 hr. interval and stops when the pH reaches around 9.5-10. The final concentration of NaOH at which this pH is achieved is dependent on the amount of DNA.

Preparation of DNA conjugated gold nanoparticles

The salt-aging method developed by Mirkin et al.[46] was used to conjugate gold nanoparticles with DNA. Thiol modified oligonucleotides 18 nt. (5'-GT AGT CGC AGA TTA TTTT/(CH2)3SH 3') were treated with TCEP (600×) overnight to cleave the disulfide bond and purified with a 3KDa Amicon Ultra-0.5 Centrifugal Filter (Millipore Sigma, Burlington, MA, USA) two times at $14000 \times g$ for 20 minutes and the concentration was measured with NanoDrop™ spectrophotometer. Then the oligonucleotides were mixed with 10nm AuNPs at a molar ratio of 660:1. After adjusting the final concentration of SDS to 0.01% w/v, a 5 M NaCl solution was added to the mixture to gradually increase the final concentration of NaCl in the mixture to 0.3 M over the course of 3 hrs. The mixture was then purified using 100K Da Amicon Ultra-0.5 Centrifugal Filter 8 times at $14000 \times g$ for 5 minutes.

DNA origami formation

The DNA origami tiles used in this study were designed with Cadnano[49] and prepared using a previously published method.[50] M13mp18 DNA (New England Biolabs) in 1× TAE-Mg²⁺ buffer (10 mM Tris base, 1 mM Ethylenediamine tetra acetic acid (EDTA), 14 mM $MgCl_2$) was mixed with 100-fold excess of short staple strands and thermally annealed from 95 °C to 20 °C in a thermocycler (BIO-RAD T100) at a rate of -1°C/minute. The folded DNA nanostructures were separated from excess DNA staple strands using a 50K Da Amicon Ultra-0.5 Centrifugal Filter. The filtration was performed at 3500 ×g for 2 mins and 5 times. Each time the solution was replenished with 1× TAE and the final concentration $MgCl_2$ was adjusted to 10 mM.

Self-assembly of nanoparticles on DNA origami

To bind the DNA conjugated gold nanoparticles and QDs to the DNA origami tile, we used a 2-step sequential annealing method. In the first step, the purified tiles were mixed with the prepared QD nanoparticles and were annealed to the tiles in 2× equimolar concentration in 1× TAE buffer and 12.5 mM $MgCl_2$. The annealing was performed in a thermocycler (Eppendorf) annealed from 41 °C to 20 °C at a rate of 1 °C/minute. In order to remove unbound or excess nanoparticles, two rounds of purification were performed using size exclusion spin columns (gel filtration purification method in SI). In the second step purified AuNP-DNA conjugates were annealed to the previously made QD-tiles in 2× equimolar concentration in 1× TAE buffer and 12.5 mM $MgCl_2$. The annealing was performed in a thermocycler (BIO-RAD T100) starting at 41°C and slowly decreased to 20 °C at a rate of -1 °C/minute. The nanoparticles-DNA origami conjugates were then purified again with size exclusion spin columns twice before TEM imaging.

Transmission electron microscopy

Transmission electron microscopy (TEM) imaging of the DNA origami and QD–DNA origami assemblies was carried out using a Talos F200C G2 transmission electron microscope operating at 200 kV. Typically, 4-5 μl of the sample was deposited onto an Argon plasma-treated formvar/carbon-coated (copper mesh) grid (Ted Pella, Inc., Redding, CA, USA; prod no. 01753-f) for up to 5 min. The excess liquid was then blotted off, and the grid was washed and stained using 2% aqueous uranyl formate solution and let dry overnight.

pH measurement

pH measurements were done using a microglass pH electrode (Fisher Scientific Accumet combination electrodes (13-620-851)and Orion star5 thermoscientific pH meter at room temperature.

DLS measurement

All dynamic light scattering (DLS) experiments were performed using ZETASIZER NANO series S90 (Malvern Panalytical). Measurements were done using a microvolume quartz cuvette (50 μL) using 632.8 nm laser with 90° scattering angle at room temperature.

Spectroscopic characterization

Concentrations of DNA origami, thiol-modified DNA, and unfunctionalized and functionalized AuNP were determined using a NanoDrop™ ND-1000 spectrophotometer (Thermo Fisher Scientific). UV-Vis spectra of unfunctionalized QDs were collected using a Perkin-Elmer Lambda 35 UV/Vis spectrophotometer using a 100 μL quartz cuvette. Fluorescence spectroscopy measurements were done using a HORIBA Instruments Inc (FL-1000) spectrometer equipped with a thermoelectrically cooled BIUV Synapse CCD detector. Although the slit width and the integration time were varied to optimize the signals, identical slit width and

integration time were used for the same set of spectra. The fluorescence intensity of functionalized QD was measured using a 50 μL Quartz 701MF sub-micro black fluorometer cuvette (Fireflysci), and the QD-Origami and QD-Au-Origami samples were run using a HORIBA Microsense (1-5 μL) cuvette.

Agarose gel electrophoresis

For DNA-functionalized nanoparticles, 0.5% agarose gels were prepared with 0.5× TBE buffer and were ran for 40 minutes with 0.5× TBE buffer at 65 volts. For origami tiles and the annealed products 1% agarose gels were prepared with 0.5× TBE/12mM $MgCl_2$, the gels were stained with fluorescent SYBR Green I (10,000×, Invitrogen) and, the sample solutions were stained with a blue loading dye (6×, NEB) before running on the gel. The running buffer for the tiles were 0.5× TBE with 5 mM $MgCl_2$ and the gels was run for 1 hour at 65 volts.

Quantification of DNA surface ligands

To quantify the number of surface DNA ligands using fluorimetry, we used a Cy5-modified oligonucleotide (Cy5-DNA) that has the same sequence as the unlabeled oligonucleotide. Ligand exchange with the fluorophore modified oligonucleotide was performed at 5 different DNA to QD molar ratios: 20, 80, 160, 320, and 640. After the completion of ligand exchange, the solutions were filtered through an ultrafiltration unit with 100 kDa MWCO to collect the DNA-functionalized QDs and remove excess unbound ssDNAs. Then the samples were treated with Dithiothreitol (DTT) overnight and incubated at 40 °C to remove the ligands from the surface of the particles. The solutions were then spun down at $14000 \times g$ to precipitate the QDs at the bottom of the test tube and the supernatants were used for fluorescent measurements.

The molar concentrations of the Cy5-DNA in the supernatants were calculated from the fluorescence intensity maxima at 560 nm and a standard linear calibration curve, which was obtained with known concentrations of Cy5-DNA in the same buffer. In the end, the average number of ssDNA strands per QD was obtained by dividing the measured concentration of fluorescent oligonucleotides by the concentration of the QDs.
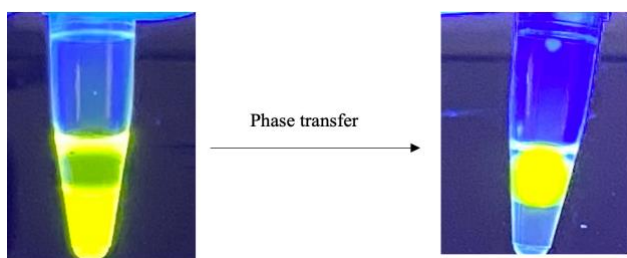
RESULTS AND DISCUSSION

Figure 1.Phase transfer of CdSe/ZnS quantum dots (QDs) from an organic phase (CH_3Cl /DMSO (100μl/50μl, bottom) to an aqueous phase (79.6 μM of 16 nt. thiol modified DNA, top). Left: 0.398 μM QDs were dissolved in the organic phase. Right: after ligand exchange, the QDs were transferred to the aqueous phase.

The direct conversion of such hydrophobic QDs into ones that are conjugated with hydrophilic DNA molecules is inherently challenging. Figure S1 shows that QDs dissolved in chloroform cannot be transferred to the aqueous phase containing DNA ligands. The hydrophobic QDs reside exclusively in the organic phase and DNA in the aqueous phase. Therefore, it is difficult for the DNA to displace the

ligands on the QDs. Even if a few DNA ligands were attached to the QDs, the DNA ligands would make the QDs unstable in the organic phase. At the same time, the QDs would remain too hydrophobic to be dispersed in the aqueous phase. To address this challenge, DMSO, which could dissolve both DNA and the octadecyl-amine ligands, was added. We found that in the presence of DMSO, these QDs migrated to the aqueous phase in as short as a few minutes (Figure 1 on the right), suggesting that hydrophilic DNAs were attached to the QDs, which made them soluble in the aqueous phase. Although the mechanistic details of the process remain to be fully explored, the likely roles for DMSO include increasing solubility of DNA ligands in the organic phase and increasing solubility of the QDs in the aqueous phase. Even if the DNA and hydrophobic QDs remain confined to their respective phases and initial ligand exchange of QDs takes place exclusively at the interface between the two phases, once an octadecylamine capped QD is conjugated with one or a few DNA ligands, it could have sufficient hydrophilic characteristics to migrate to the aqueous phase, which contains DMSO that stabilizes the amphiphilic QD. Once such QDs are in the aqueous phase, ligand exchange would accelerate. With the initial success in ligand exchange, we studied how the DNA/QD ratio and utilization of a strong base affect the size, stability, and photoluminescence of the QD-DNA conjugates.

The roles of NaOH addition

Previous reports suggested that the thiol groups need to be deprotonated for facile binding to QDs.[51] As TCEP was added to prevent surface etching of the QDs, the pH of the as-prepared aqueous phase was about 3. At this pH, the thiol groups of the ssDNA ligands are protonated, making ligand exchange challenging. To promote the conjugation of thiol-modified oligonucleotides to the QDs, we added 200 mM NaOH to the aqueous phase in a dropwise fashion to increase the pH up to 9-10, which is close to the pk_a of thiol modified DNA. The effect of base addition was monitored with dynamic light scattering and fluorescence spectroscopy. Figure 2 shows that when ligand exchange was carried out at pH ~ 5, the hydrodynamic sizes were in the range of hundreds of nanometers for both [DNA]/[QD] molar ratios, 320 and 640, suggesting significant agglomeration of these QDs. As more NaOH was added and the pH raised, the hydrodynamic sizes declined to tens of nanometers, indicating that the QDs become more dispersed. At higher pH values, more thiol-modified DNAs became deprotonated and the ligand exchange with octadecyl amine was facilitated, diminishing aggregation of the QDs. While this trend was observed for both [DNA]/[QD]=320 and [DNA]/[QD]=640 samples, the samples with more DNA showed smaller hydrodynamic sizes, suggesting that the DNA ligands at a higher concentration formed a denser DNA shell around the QDs and reduced aggregation.

Fluorescence spectroscopy was also used to monitor the reaction progression. The fluorescence spectra of samples with different [DNA]/[QD]:160, 320 and, 640 were measured at pH ~5, ~7 and ~9. As NaOH was added to the reaction mixture to increase the pH, the fluorescence of

these QD-DNA conjugates was enhanced for all three molar ratios (Figure 2c).

Another possible role of the NaOH addition in the ligand exchange reaction is raising the ionic strength. The repulsion between the negatively charged DNA ligands makes it difficult to conjugate DNA to nanoparticles at high surface densities. As the concentration of Na^+ is increased in the solution, the electrostatic repulsion between the nanoparticles is more screened, allowing more DNA to bind to the QDs. This role is similar to the role that NaCl played in the salt aging method to functionalize gold nanoparticles with DNA, where the ionic strength is gradually increased to allow more DNA ligands to bind.
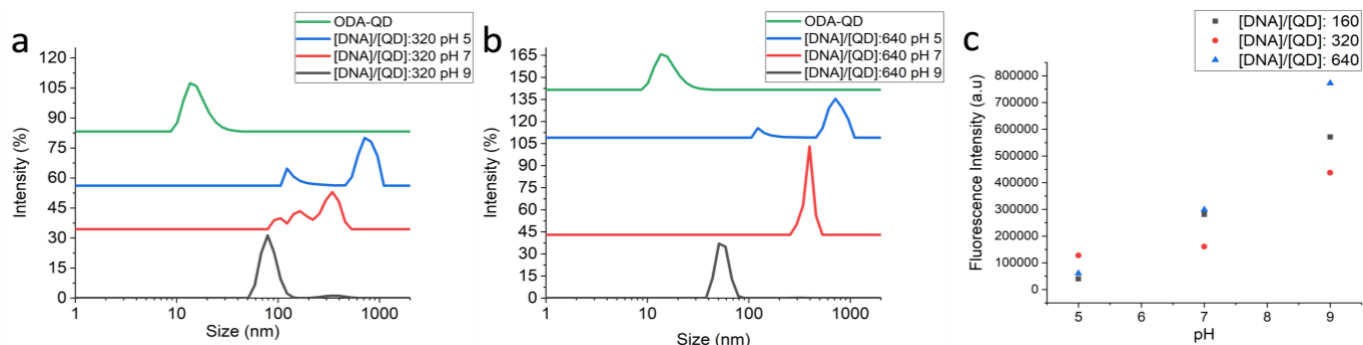

Figure 2.Size distributions of octadecylamine-QDs as well as QD-DNA conjugates that were prepared under different pHs and two, (a)320 and (b) 640. (c) Peak fluorescence intensities (λmax= 560 nm) of the QD-DNA conjugates.

Evidence for this role is that the addition of base should be completed in a stepwise manner over the course of a few hours. Rapid addition of NaOH within a few min produced precipitates visible under the UV light (Figure S2). While the electrostatic repulsion between DNA needs to be reduced for facile conjugation, QDs in the aqueous phase are stabilized by electrostatic repulsions. When the ionic strength is increased too quickly, the repulsive interactions between QDs that are not covered with enough DNA ligands may be reduced too quickly, leading to irreversible aggregation. Also, to understand the roles of pH and ionic strength, NaCl was used instead of NaOH in the ligand exchange process. Figure S6 shows that the resulting QDs were heavily aggregated, suggesting that a higher ionic strength alone is not sufficient to ensure facile ligand exchange with thiolated DNA. A sufficiently high pH is also important for successful conjugation of the hydrophobic QDs with thiolated DNA.

The effect of DNA/QD ratio

Figure 3a shows that the QDs were transferred to the aqueous phase at all [DNA]/[QD] ratios tested. Under UV illumination, the bottom organic layer no longer showed fluorescence. Instead, the fluorescence originated exclusively from the top aqueous layer. However, there are visible differences in the aqueous phase. The samples prepared at lower [DNA]/[QD] displayed lower fluorescence and were less uniform. Dynamic light scattering (DLS) was also used to measure the hydrodynamic diameter of the QD-DNA conjugates prepared at different DNA/QD molar ratios (Figure 3c). The larger hydrodynamic sizes at smaller molar ratios suggest agglomeration at lower DNA concentrations. As the DNA/QD molar ratio increased, the hydrodynamic sizes of the resulting QD-DNA conjugates declined. At 640× DNA, the size is 30 nm, which is close to 29 nm, the calculated physical dimension of the QD-DNA conjugate assuming the average length of a stretched single- stranded DNA ligand to be 10.8nm [52] and the diameter of the QD to be 7 nm. As the scattered intensity scales with the hydrodynamic size to the sixth power, even a small fraction of larger aggregates could dominate the intensity distribution. Therefore, the observed size distribution shows that 640× DNA can form well-dispersed QD-DNA conjugates of the expected dimension with minimal aggregation.

To further assess the efficiency of the phase transfer, the QDs transferred to the aqueous phase were characterized using agarose gel electrophoresis (1% agarose, 1× TAE (40 mM Tris base, 20 mM Acetic acid, 1 mM EDTA), 11 mM $MgCl_2$ buffer; 6.5 V/cm for 1.5 hr.). The bands at the bottom correspond to the free DNA ligands, and the bands just below the wells correspond to QDs that are conjugated with DNA (Figure 3b). The lower mobility bands provide additional confirmation of the success of the ligand exchange reaction: unlike the QDs with the neutral hydrophobic ligands, the QDs functionalized with DNA are negatively charged and can migrate out of the wells. The faint band for the 20× DNA sample suggests that the ligand exchange was incomplete, and many of the particles were trapped in the interface between the two phases rather than migrating to the aqueous phase.
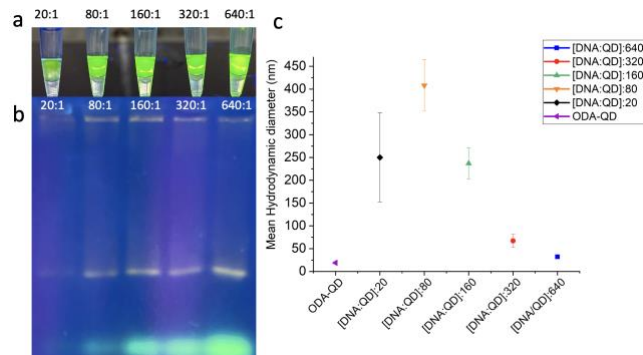

Figure 3. (a)Phase transfer products for different molar ratios of DNA/QD at pH ~9.5-10, the picture was captured under 302 nm UV illumination (b) Agarose gel image of QD-DNA

conjugates formed at different molar ratios of DNA/QD. SYBR Green II was used to stain the ssDNA. (c) Hydrodynamic diameter of DNA functionalized QD with 3' end poly T, thiol modified DNA with different [DNA]/[QD]. NaOH was added to all these samples to achieve a final pH of 9.5-10.

We note that the measured hydrodynamic size does not monotonically decline with increasing DNA/ QD molar ratio. Specifically, the QD sample prepared with 20x DNA shows smaller hydrodynamic sizes compared to QD samples with 80× DNA and 160× DNA (Figure 3c). This anomaly may be understood by considering that at 20x DNA, most particles were trapped at the organic/water interface and only a small fraction of them successfully migrated to the aqueous phase (Figures 3a). The QDs that migrated to the aqueous phase were less agglomerated than QDs conjugated under 80x and 160x DNA, which were able to transfer a higher fraction of the aggregated QDs to the aqueous phase. The trends shown in Figure 3 and Figure 3c confirm that as the DNA/QD was increased, more QD nanoparticles left the two-phase interface and got dispersed in the aqueous solution. The more ligands available for this transition, the less aggregation is obtained (Figure 3c). The mono-dispersity of the QD-DNA conjugates were also confirmed with transmission electron microscopy (TEM) (Figure 4). Our TEM measurements show that the average size of the QD-DNA conjugates, 8.4±1 nm, is virtually identical to that of original hydrophobic QDs, 7.5±1 nm.
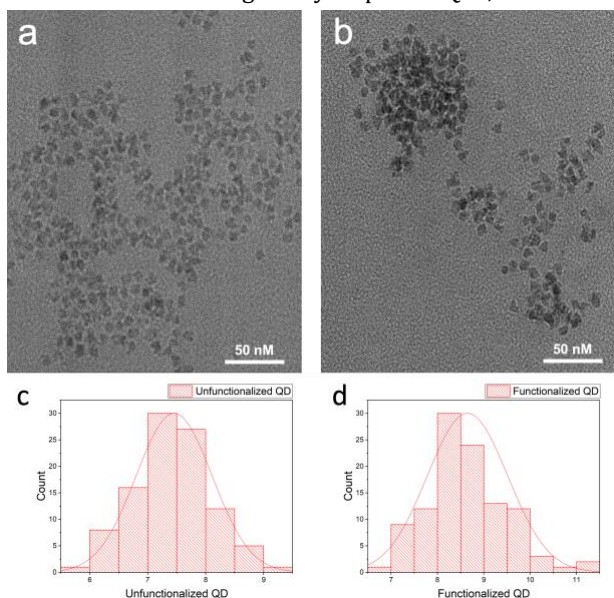

Figure 4.TEM image of (a),1-octadecylamine capped QDs and (c), their size distribution. TEM image of (b) QD-DNA conjugates (prepared with molar ratio [DNA]/[QD]:640) and (d) their size distribution.

While mono-dispersity is an important criterion for successful QD bioconjugation, the QDs must also retain photoluminescence after conjugation. Therefore, we measured the fluorescence spectra of the QDs conjugated under different conditions (Figure 5). Our measurement shows that the overall, higher DNA ratios produce QD-DNA conjugates with higher photoluminescence. The lower photoluminescence with 20x DNA and 80x DNA likely is a consequence of the incomplete transfer of the nanoparticles to the aqueous phase at these lower DNA concentrations. As many of the QDs were not conjugated with enough DNA ligands to be water-soluble, they were trapped at the interface between two phases. Moreover, many of the QDs that were transferred to the aqueous phase were in the aggregated form, further diminishing photoluminescence. The QDs that are conjugated with 640x DNA show the highest photoluminescence. Also, small red shifts in the peak emission up to 2-3 nm were observed in samples with lower DNA/QD ratios, such as 20 and 80 (Figure S5). While the small magnitude of the red shift appears to contradict the DLS results (Figure 2) suggesting significant aggregation, DLS is substantially more sensitive to aggregation than fluorescence spectroscopy, with the scattered light intensity being proportional to the sixth power of the hydrodynamic size.[53] Even a small fraction of large aggregates may dominate the intensity distribution. The lack of a significant red shift in emission for QDs prepared at low DNA/QD ratios, in combination with increased DLS hydrodynamic sizes, suggests that a relatively small fraction of QDs aggregated and fluorescence emission was dominated by isolated QDs. While aggregation of QDs can shift emission to longer wavelengths, the small red shift may also originate from the changes in the local environment due to ligand exchange.[54-56] For example, at a low ligand loading, the ligand surface density is less uniform, generating local electric fields that could stabilize the exciton and shift the emission peak to a longer wavelength.

The intensity of photoluminescence of the 640x DNA conjugated QDs is similar to that of Octadecyl amine coated QDs at identical concentration, excitation wavelength, and excitation power, suggesting that they have similar quantum yields (Figure S14). Taking into account the different refractive indices of the solvents,[57] the quantum yield of the DNA conjugated QD is about 100±16% of that for octadecylamine capped QDs. As the nanoparticles are protected by a denser layer of DNA ligands, aggregation and surface etching, which can diminish the emission, are minimized. Our observation is consistent with previous studies showing that when QDs are fully protected with the surface ligands, they are monodisperse and their photoluminescence is preserved.[17, 36] We also note that the intensity does not strictly increase monotonically with increasing DNA/QD. In fact, 160x DNA leads to the higher intensity that 320x DNA. While the trend remains to be fully understood, a similar trend was observed in a previous report, which suggests that certain forms of aggregation may lead to higher photoluminescence. [13]
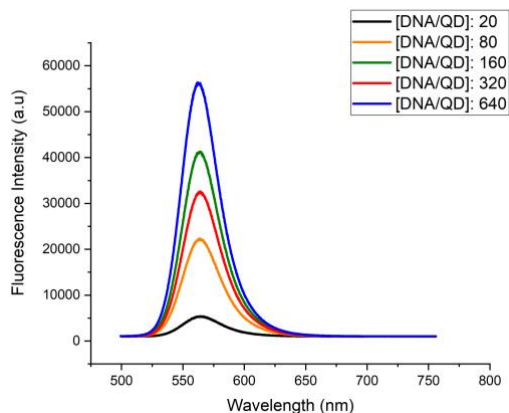
Figure 5. Fluorescence spectra of QD-DNA conjugates excited at 470 nm. The samples with different [DNA]/[QD] ratios were prepared to have the same final QD concentrations as measured by UV-Vis. NaOH was gradually added to each of these samples to achieve a final pH of 9.5-10.

Quantification of the DNA surface ligands

The preceding section provides indirect evidence supporting that more DNA ligands are attached to the QDs as the DNA/QD molar ratio used for ligand exchange increases. Direct quantification of the surface ligands is desirable for a better understanding of the ligand exchange process and for applications that require knowledge of the ligand surface density. Therefore, we used a Cy5-modified oligonucleotide (Cy5-DNA) that shared the same sequence of the dye-free DNA ligand to perform ligand exchange/phase transfer. After the QD-Cy5-DNA conjugates were purified, the Cy5-DNA ligands were desorbed by addition of DTT, separated from QDs using centrifugation and quantified with fluorimetry using a method previously developed to quantify DNA loading on nanoparticles (Experimental Section). Figure 6 confirms that as more DNA is added for ligand exchange, the average number of bound DNA ligands per QD increases. With of 20× thiolated DNA, on average only 1.6±0.4 DNA molecules are attached to a QD. As a significant amount of octadecylamine remains on the QDs, such QDs display low stability. The significantly lower fluorescence of the 20× thiolated DNA in Figure 3b shows that a significant fraction of the QDs were trapped within the well. Future LC-MS experiments could help quantify the loading of the hydrophobic ligands on the QDs and provide additional insight into the ligand exchange process. For the 640× DNA, the average number of DNA ligands reaches 9.6±0.7. The trend tracks increasing mono-dispersity and photoluminescence of these QD-DNA conjugates. The surface density of DNA on QD is calculated to be 0.062 molecule/nm^2, which is somewhat lower than but still comparable to the typical DNA loading achieved for gold nanoparticles, ~ 0.1 molecule/nm^2. [46]
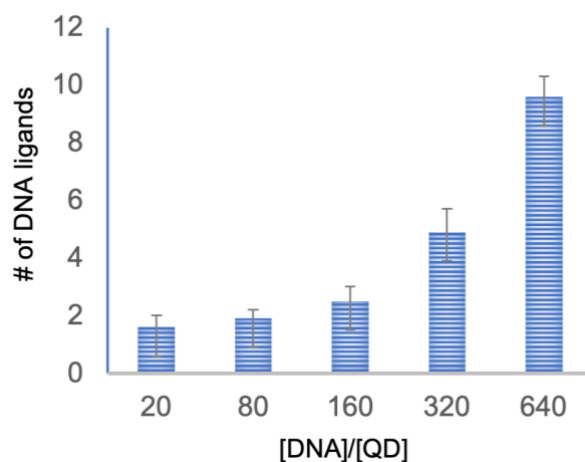

Figure 6. DNA loading as a function of [DNA]/[QD].

Co-assembly of QDs and gold nanoparticles on a DNA origami template

The unique photophysical properties of QDs, such as tunable emission, wide bandgaps and narrow emission wavelength ranges, make them valuable for energy transfer studies and biosensor designs.[21, 34] Since the energy transfer efficiency is distance-dependent, it is important to precisely control the distance between the nanoparticles as well as the number of the interacting particles. DNA-nanoparticle conjugates can site-specifically bind to self-assembled templates, such as DNA origami[58, 59] and DNA bricks.[41] Capture strands on these templates can hybridize with DNA ligands on nanoparticles to arrange these nanoparticles in sophisticated arrangements with nanometer precision. While there have been a large number of studies that use DNA to direct the self-assembly of gold nanoparticles,[59, 60] fewer analogous studies for QDs have been carried out due to the difficulty in forming QD-DNA conjugates with sufficient colloidal stability under high salt conditions, small sizes, and high photoluminescence. Among those studies, many of them relied on streptavidin-biotin interactions to bind streptavidin-conjugated QDs to biotinylated DNA templates.[61, 62] Unlike those that use base pairing for nanoparticle binding, methods that rely on the streptavidin-biotin interaction to place nanoparticles lack diversity of specific interactions that are needed to organize nanoparticles of different size/shapes/compositions on the same template. To evaluate the utility of our method for DNA-directed self-assembly of QDs, we used DNA origami as a template to self-assemble a heterodimer that consists of a DNA conjugated gold nanoparticle and a DNA conjugated QD.

The schematic of the DNA-directed self-assembly method is shown in Figure 7a. The capture strands at the designed locations on the DNA origami tile can bind the DNA functionalized nanoparticles on the tile, with a predicted center-to-center distance of 22 nm (Figure S15). The self-assembly product of this experiment was then characterized with TEM at 200 kV (Figure 7d) and agarose gel electrophoresis at 65 volts and 0.5× TAE/12 mM MgCl$_2$ (Figure 7c). For the TEM imaging, Uranyl formate 2% was used to stain the DNA origami for better resolution (Figure 7d). The rectangular shapes shown in the image are the

DNA tiles with the two nanoparticles (QD and Au) annealed to them. The smaller particles correspond to QDs, and the larger ones correspond to Au nanoparticles. The measured center-to center distance is 20±2 nm, which is close to the predicted distance of 22 nm. 68% of the DNA origami tiles have captured a nanoparticle dimer. 31 % of the tiles only have a single nanoparticle. Additional TEM images are provided in Figure S11. AFM images of tiles with a QD and tiles with heterodimer are included in Figures S12 and S13 respectively. In the AFM images, the QDs and AuNPs can be distinguished by their topographical heights. The QDs have an average height of 5 nm ± 2 nm and the AuNPs have an average height of 12.2 nm ± 0.8 nm.

Gel electrophoresis results in Figure 7b and Figure 7c confirm that both the QD and the AuNP successfully bound to the DNA origami tiles. The free QD-DNA conjugates (first lane from the left) run faster compared to QD-DNA conjugates that are annealed with the tile (second lane from the left, Figure 7b), suggesting successful binding of QDs to the DNA origami tile. A picture of the same gel was taken under white light illumination to better visualize the mobility of Au NPs compared to Au NPs annealed to the tile (Figure 7c). The fourth lane shows the mobility of Au NPs and they run faster on the gel compared to Au NPs when annealed on the tile (the third lane from the right). The annealed Au nanoparticles in the third lane show two bands; the band on the bottom corresponds to free excess Au nanoparticles and the band on the top corresponds to the Au NPs pinned on the origami tile.
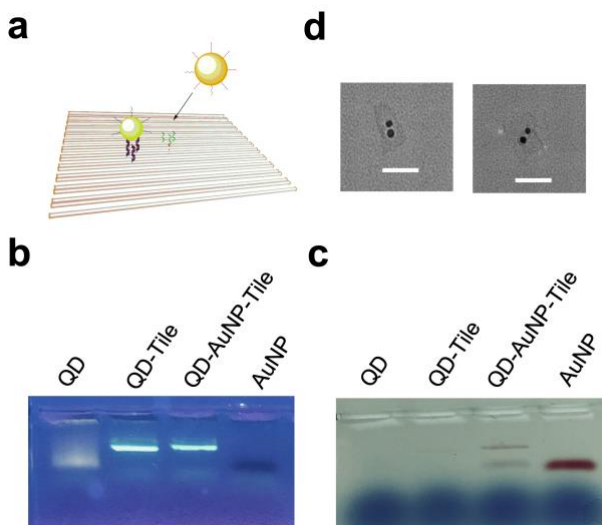
Figure 7. (a) Schematic of annealing of nanoparticles to the origami tile. Binding of Au (dark yellow) and QD (green) onto DNA origami tile. Complementary strands on QD hybridize with capture strands on DNA tile. (b) Agarose gel image of functionalized nanoparticles and annealing products under 302 nm UV light. (c) Agarose gel image under white light illumination. (d)TEM image of self-assembled Au and QD on origami tile. Scale bar is 50 nm.

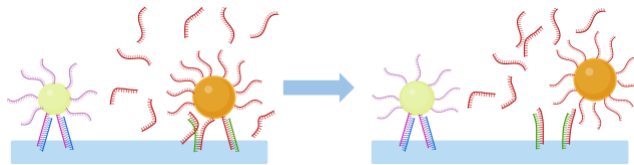## Application of QD-AuNP heterodimers for energy transfer studies

Figure 8. Schematic showing how addition of excess DNA ligand (a) causes displacement of AuNP (dark yellow) from the origami tile (b). For simplicity, a halo around the nanoparticle represents surface ligands.

Energy transfer between nanoparticles in close proximity is extremely sensitive to interparticle distances.[34] The use of DNA origami as a breadboard provides the ability for site-specific binding of nanoparticles.[7, 40, 63] Here we have performed a proof-of-principle experiment that used the self-assembled heterodimers for energy transfer studies and biosensor design. We designed a simple experiment to study how the binding of AuNP to the origami and its displacement affects the PL of the QDs (Figure 8). After dimer formation, excess ligands that are complementary to the capture strands for the AuNP were added to dissociate the AuNP from the DNA origami tile and consequently increase the distance between the QD and AuNP. Fluorescence spectra before and after the displacement were measured to study the effect of energy transfer.

QDs and AuNPs were annealed to the DNA origami respectively, to form the dimer structures, which were then purified using size exclusion spin columns[51] to remove unbound nanoparticles. The gel results in Figure 9a show that the nanoparticles were successfully bound to the origami tile (AuNP-QD-tiles): the top band lines up to the band for the tiles, and the bottom band shows the presence of excess unbound AuNPs. After adding the excess ligands at a concentration of 80 μM (520 times in excess relative to the amount of the origami tiles), the top red band disappeared (AuNP displacement) and the bottom band lined up with the band for unbound AuNPs on the left, showing that the AuNP dissociated from the tile. Lastly, in order to measure the quenching effect of AuNP on QD photoluminescence, the fluorescence intensities at 560 nm of QD-Tile, AuNP-QD-tile and tiles after displacement of AuNPs were measured at an excitation wavelength of 470 nm (Figure 9b). A comparison of the red curve representing the tiles with a QD and the blue curve representing tiles with a heterodimer shows that when the AuNP is bound to the QD-tile, the PL at 560 nm decreases by 40%. After ligands were added to displace the gold nanoparticles (dotted curve, AuNP Displacement), the PL intensity almost fully recovered (Figure 9b). Our study shows that after AuNP displacement the fluorescence intensity is enhanced by 39±5% on average (Figure S14).
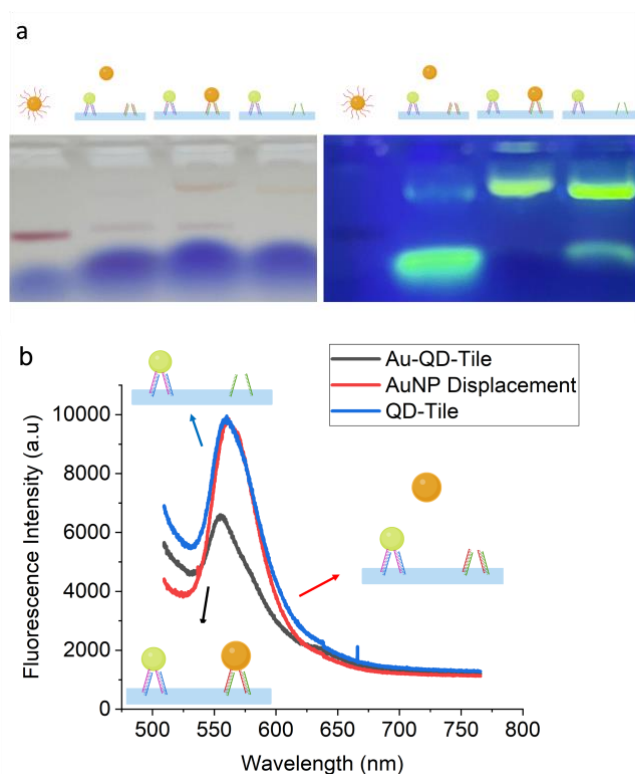
Figure 9. (a) Agarose gel (1% with 0.5x TBE/12 mM MgCl2 running buffer) left to right; functionalized AuNP (AuNP), displacement of gold nanoparticles by adding excess ligand (AuNP displacement), Tile. (b)Quenching effect of AuNPs on QDs bound to DNA origami; PL of QD-Tile (red), Au-QD-Tile(blue) and Au-QD-Tile after addition of ligands to displace AuNPs (AuNP Displacement, dashed black).

Energy transfer is known to be highly distance sensitive. The average surface-to-center distance between the AuNP and the QD increased from ~15 nm to a few hundred nanometers, which is too large to enable significant energy transfer. Therefore, these unbound AuNPs can no longer effectively quench the PL of the QDs. It should be noted that the PL near 525 nm is more complex. The QD-tiles sample has the highest PL intensity, and the other two samples have lower intensities. As the wavelength is near the surface plasmon resonance of the AuNPs, factors contributing to the differences include direct absorption, surface quenching, metal surface enhanced radiative decay.[64] While a more systematic study is needed to elucidate the complex trend, the results nevertheless have shown that our method produces QD-DNA conjugates with small sizes that make them suitable for energy transfer studies. And the increases in PL upon addition of DNA suggests that the heterodimer on DNA origami provides a signal transduction mechanism for detection of nucleic acids.

CONCLUSIONS AND OUTLOOK

We have shown that our one-step ligand exchange method can form compact, monodisperse, and bright QD-DNA conjugates from commonly available hydrophobic quantum dots. These QD-DNA conjugates have sufficient colloidal stability to bind to a DNA origami template at prescribed separations from a gold nanoparticle, enabling investigation of energy transfer between QDs and AuNPs. This study focused on two key parameters, pH and DNA/QD ratio. Our simple method can be extended to other QDs with different hydrophobic ligands and compositions. Multidentate ligands that bind to QDs more strongly may be used to further enhance the stability of these QD-DNA conjugates.[65, 66] Like other ligand exchange methods,[23] our method requires a relatively large excess of DNA ligands to achieve high DNA loading on the QDs. Future studies that systematically explore the effects of QD composition, size, length of DNA, reaction time and use stronger binding groups such as dithiols would provide additional insights into the ligand exchange process and increase its efficiency.

With further optimizations, our designer nanostructures may serve as a signal-on sensor for ultra-sensitive detection of nucleic acids and other biomarkers[67] as the PL signal can report the presence of nucleic acids or other biomarkers that displace the AuNPs from the DNA origami tile (Figure 7). The sensitivity may be substantially enhanced by improving the quenching efficiency of the heterodimers and introducing a toehold to accelerate strand displacement. In addition to forming simple dimer structures, these QD-DNA conjugates may be assembled into superlattices as well as complex clusters with novel emergent properties. Therefore, this approach has the potential to make QDs more ubiquitous components in DNA mediated self-assembly.

ASSOCIATED CONTENT

Supporting Information

This material is available free of charge via the Internet on the ACS Publications website at Applied materials and interfaces, DNA origami tile sequences, design of capture strands, Fluorescence spectra, TEM of origami tiles. Calibration curve spectra.

AUTHOR INFORMATION

Corresponding Author

Tao Ye – *Chemistry and Biochemistry, University of California, Merced, California, 95343, United States*; orcid.org/0000-0001-8615-3275; Email: tao.ye@ucmerced.edu

Author Contributions

P.R. and T.Y conceived the experiments. P.R., M.G., Y.Z., and Y.L. performed the experiments. The manuscript was written through contributions of all authors. All authors have given approval to the final version of the manuscript.

ABBREVIATIONS

QD, Quantum Dot; ssDNA, single stranded DNA; TEM, transmission electron microscopy.

REFERENCE

1.   Raino, G.; Becker, M. A.; Bodnarchuk, M. I.; Mahrt, R. F.; Kovalenko, M. V.; Stoferle, T., Superfluorescence from Lead Halide Perovskite Quantum Dot Superlattices. *Nature* **2018,** *563*, 671-675.

2.   Kagan, C.; Murray, C.; Nirmal, M.; Bawendi, M., Electronic Energy Transfer in Cdse Quantum Dot Solids. *Phys. Rev. Lett.* **1996,** *76*, 1517-1520.

3.   Chon, J. W. M.; Moser, J.; Gu, M. In *Use of Semiconductor Nanocrystals for Spectrally Encoded High-Density Optical Data Storage*, International Symposium on Optical Memory and Optical Data Storage, Honolulu, Hawaii, 2005/07/10; Optica Publishing Group: Honolulu, Hawaii, 2005; p MP13.

4.   Lan, X.; Masala, S.; Sargent, E., Charge-Extraction Strategies for Colloidal Quantum Dot Photovoltaics. *Nat. Mater.* **2014,** *13*, 233-240.

5.   Du, K.; Ko, S.; Gallatin, G.; Yoon, H.; Liddle, J.; Berglund, A., Quantum Dot-DNA Origami Binding: A Single Particle, 3d, Real-Time Tracking Study. *Chem. Commun.* **2013,** *49*, 907-909.

6.   Krovi, H., Models of Optical Quantum Computing. *Nanophotonics* **2017,** *6*, 531-541.

7.   Bui, H.; Onodera, C.; Kidwell, C.; Tan, Y.; Graugnard, E.; Kuang, W.; Lee, J.; Knowlton, W. B.; Yurke, B.; Hughes, W. L., Programmable Periodicity of Quantum Dot Arrays with DNA Origami Nanotubes. *Nano Lett.* **2010,** *10*, 3367-3372.

8.   Huang, D.; Freeley, M.; Palma, M., DNA-Mediated Patterning of Single Quantum Dot Nanoarrays: A Reusable Platform for Single-Molecule Control. *Sci. Rep.* **2017,** *7*, 45591.

9.   Mathur, D.; Samanta, A.; Oh, E.; Díaz, S. A.; Susumu, K.; Ancona, M. G.; Medintz, I. L., Quantum Dot Encapsulation Using a Peptide-Modified Tetrahedral DNA Cage. *Chem. Mater.* **2017,** *29*, 5762-5766.

10.   Bilan, R.; Nabiev, I.; Sukhanova, A., Quantum Dot-Based Nanotools for Bioimaging, Diagnostics, and Drug Delivery. *ChemBioChem* **2016,** *17*, 2103-2114.

11.   Medintz, I. L.; Uyeda, H. T.; Goldman, E. R.; Mattoussi, H., Quantum Dot Bioconjugates for Imaging, Labelling and Sensing. *Nat. Mater.* **2005,** *4*, 435-446.

12.   Cheng, Y.; Ling, S. D.; Geng, Y.; Wang, Y.; Xu, J., Microfluidic Synthesis of Quantum Dots and Their Applications in Bio-Sensing and Bio-Imaging. *Nanoscale Advances* **2021,** *3*, 2180-2195.

13.   Hines, M. A.; Guyot-Sionnest, P., Synthesis and Characterization of Strongly Luminescing Zns-Capped Cdse Nanocrystals. *J. Phys. Chem.* **1996,** *100*, 468-471.

14.   Liu, H.; Owen, J.; Alivisatos, A., Mechanistic Study of Precursor Evolution in Colloidal Group Ii-Vi Semiconductor Nanocrystal Synthesis. *J. Am. Chem. Soc.* **2007,** *129*, 305-312.

15.   Yin, Y.; Alivisatos, A. P., Colloidal Nanocrystal Synthesis and the Organic-Inorganic Interface. *Nature* **2005,** *437*, 664-670.

16.   Murray, C. B.; Norris, D. J.; Bawendi, M. G., Synthesis and Characterization of Nearly Monodisperse Cde (E = Sulfur, Selenium, Tellurium) Semiconductor Nanocrystallites. *J. Am. Chem. Soc.* **1993,** *115*, 8706-8715.

17.   Lees, E. E.; Nguyen, T. L.; Clayton, A. H. A.; Mulvaney, P.; Muir, B. W., The Preparation of Colloidally Stable, Water-Soluble, Biocompatible, Semiconductor Nanocrystals with a Small Hydrodynamic Diameter. *ACS Nano* **2009,** *3*, 1121-1128.

18.   Uyeda, H.; Medintz, I.; Jaiswal, J.; Simon, S.; Mattoussi, H., Synthesis of Compact Multidentate Ligands to Prepare Stable Hydrophilic Quantum Dot Fluorophores. *J. Am. Chem. Soc.* **2005,** *127,* 3870-3878.

19.   Lin, C.; Sperling, R.; Li, J.; Yang, T.; Li, P.; Zanella, M.; Chang, W.; Parak, W., Design of an Amphiphilic Polymer for Nanoparticle Coating and Functionalization. *Small* **2008,** *4*, 334-341.

20.   Medintz, I. L.; Mattoussi, H., Quantum Dot-Based Resonance Energy Transfer and Its Growing Application in Biology. *Physical Chemistry Chemical Physics* **2009,** *11*, 17-45.

21.   Clapp, A. R.; Medintz, I. L.; Mattoussi, H., Forster Resonance Energy Transfer Investigations Using Quantum-Dot Fluorophores. *Chemphyschem* **2006,** *7*, 47-57.

22.   Clapp, A.; Medintz, I.; Mauro, J.; Fisher, B.; Bawendi, M.; Mattoussi, H., Fluorescence Resonance Energy Transfer between Quantum Dot Donors and Dye-Labeled Protein Acceptors. *J. Am. Chem. Soc.* **2004,** *126*, 301-310.

23.   Mitchell, G. P.; Mirkin, C. A.; Letsinger, R. L., Programmed Assembly of DNA Functionalized Quantum Dots. *J. Am. Chem. Soc.* **1999,** *121*, 8122-8123.

24.   Su, S.; Fan, J.; Xue, B.; Yuwen, L.; Liu, X.; Pan, D.; Fan, C.; Wang, L., DNA-Conjugated Quantum Dot Nanoprobe for High-Sensitivity Fluorescent Detection of DNA and Micro-Rna. *ACS Appl Mater Inter* **2014,** *6*, 1152-1157.

25.   Shen, H. Y.; Jawaid, A. M.; Snee, P. T., Poly(Ethylene Glycol) Carbodiimide Coupling Reagents for the Biological and Chemical Functionalization of Water-Soluble Nanoparticles. *ACS Nano* **2009,** *3*, 915-923.

26.   Diaz, S. A.; Gillanders, F.; Jares-Erijman, E. A.; Jovin, T. M., Photoswitchable Semiconductor Nanocrystals with Self-Regulating Photochromic Forster Resonance Energy Transfer Acceptors. *Nature Communications* **2015,** *6*, 6036.

27.   Sapsford, K. E.; Algar, W. R.; Berti, L.; Gemmill, K. B.; Casey, B. J.; Oh, E.; Stewart, M. H.; Medintz, I. L., Functionalizing Nanoparticles with Biological Molecules: Developing Chemistries That Facilitate Nanotechnology. *Chem. Rev.* **2013,** *113*, 1904-2074.

28.   Ding, Y.; Bi, J.; Du, B.; Hu, X.; Liu, F., Aqueous Synthesis of Glutathione Capped Znse Nanocrystals: Synthesis and Optical Properties. *Mater. Res. Innovations* **2013,** *17*, 142-147.

29.   Han, H.; Zylstra, J.; Maye, M. M., Direct Attachment of Oligonucleotides to Quantum Dot Interfaces. *Chem. Mater.* **2011,** *23*, 4975-4981.

30.   Green, C. M.; Hastman, D. A.; Mathur, D.; Susumu, K.; Oh, E.; Medintz, I. L.; Díaz, S. A., Direct and Efficient Conjugation of Quantum Dots to DNA Nanostructures with Peptide-Pna. *ACS Nano* **2021,** *15*, 9101-9110.

31.   Macfarlane Robert, J.; Lee, B.; Jones Matthew, R.; Harris, N.; Schatz George, C.; Mirkin Chad, A., Nanoparticle Superlattice Engineering with DNA. *Science* **2011,** *334*, 204-208.

32.   Shen, J. L.; Tang, Q.; Li, L.; Li, J.; Zuo, X. L.; Qu, X. M.; Pei, H.; Wang, L. H.; Fan, C. H., Valence-Engineering of Quantum Dots Using Programmable DNA Scaffolds. *Angewandte Chemie-International Edition* **2017,** *56*, 16077-16081.

33.   Farlow, J.; Seo, D.; Broaders, K.; Taylor, M.; Gartner, Z.; Jun, Y., Formation of Targeted Monovalent Quantum Dots by Steric Exclusion. *Nat. Methods* **2013,** *10*, 1203-1205.

34.   Samanta, A.; Zhou, Y. D.; Zou, S. L.; Yan, H.; Liu, Y., Fluorescence Quenching of Quantum Dots by Gold Nanoparticles: A Potential Long Range Spectroscopic Ruler. *Nano Lett.* **2014,** *14*, 5052-5057.

35.   Zhang, T.; Liedl, T., DNA-Based Assembly of Quantum Dots into Dimers and Helices. *Nanomaterials* **2019,** *9*, 339.

36.   Deng, Z. T.; Samanta, A.; Nangreave, J.; Yan, H.; Liu, Y., Robust DNA-Functionalized Core/Shell Quantum Dots with Fluorescent Emission Spanning from Uv-Vis to near-Ir and Compatible with DNA-Directed Self-Assembly. *J. Am. Chem. Soc.* **2012,** *134*, 17424-17427.

37.   Samanta, A.; Deng, Z. T.; Liu, Y., Infrared Emitting Quantum Dots: DNA Conjugation and DNA Origami Directed Self-Assembly. *Nanoscale* **2014,** *6*, 4486-4490.

38. Tikhomirov, G.; Hoogland, S.; Lee, P. E.; Fischer, A.; Sargent, E. H.; Kelley, S. O., DNA-Based Programming of Quantum Dot Valency, Self-Assembly and Luminescence. *Nature Nanotechnology* **2011,** *6*, 485-490.

39. Zheng, J. W.; Constantinou, P. E.; Micheel, C.; Alivisatos, A. P.; Kiehl, R. A.; Seeman, N. C., Two-Dimensional Nanoparticle Arrays Show the Organizational Power of Robust DNA Motifs. *Nano Lett.* **2006,** *6*, 1502-1504.

40. Kuzyk, A.; Schreiber, R.; Fan, Z. Y.; Pardatscher, G.; Roller, E. M.; Hogele, A.; Simmel, F. C.; Govorov, A. O.; Liedl, T., DNA-Based Self-Assembly of Chiral Plasmonic Nanostructures with Tailored Optical Response. *Nature* **2012,** *483*, 311-314.

41. Ke, Y. G.; Ong, L. L.; Sun, W.; Song, J.; Dong, M. D.; Shih, W. M.; Yin, P., DNA Brick Crystals with Prescribed Depths. *Nature Chemistry* **2014,** *6*, 994-1002.

42. Sharma, J.; Chhabra, R.; Cheng, A.; Brownell, J.; Liu, Y.; Yan, H., Control of Self-Assembly of DNA Tubules through Integration of Gold Nanoparticles. *Science* **2009,** *323*, 112-116.

43. Levicky, R.; Herne, T. M.; Tarlov, M. J.; Satija, S. K., Using Self-Assembly to Control the Structure of DNA Monolayers on Gold: A Neutron Reflectivity Study. *J. Am. Chem. Soc.* **1998,** *120*, 9787-9792.

44. Park, S. J.; Lazarides, A. A.; Storhoff, J. J.; Pesce, L.; Mirkin, C. A., The Structural Characterization of Oligonucleotide-Modified Gold Nanoparticle Networks Formed by DNA Hybridization. *J. Phys. Chem. B* **2004,** *108*, 12375-12380.

45. Storhoff, J.; Elghanian, R.; Mucic, R.; Mirkin, C.; Letsinger, R., One-Pot Colorimetric Differentiation of Polynucleotides with Single Base Imperfections Using Gold Nanoparticle Probes. *J. Am. Chem. Soc.* **1998,** *120*, 1959-1964.

46. Hurst, S.; Lytton-Jean, A.; Mirkin, C., Maximizing DNA Loading on a Range of Gold Nanoparticle Sizes. *Anal. Chem.* **2006,** *78*, 8313-8318.

47. Li, Z. T.; Cheng, E. J.; Huang, W. X.; Zhang, T.; Yang, Z. Q.; Liu, D. S.; Tang, Z. Y., Improving the Yield of Mono-DNA-Functionalized Gold Nanoparticles through Dual Steric Hindrance. *J. Am. Chem. Soc.* **2011,** *133*, 15284-15287.

48. Wang, W.; Guo, Y.; Tiede, C.; Chen, S.; Kopytynski, M.; Kong, Y.; Kulak, A.; Tomlinson, D.; Chen, R.; McPherson, M.; Zhou, D., Ultraefficient Cap-Exchange Protocol to Compact Biofunctional Quantum Dots for Sensitive Ratiometric Biosensing and Cell Imaging. *ACS Appl Mater Inter* **2017,** *9*, 15232-15244.

49. Douglas, S. M.; Marblestone, A. H.; Teerapittayanon, S.; Vazquez, A.; Church, G. M.; Shih, W. M., Rapid Prototyping of 3d DNA-Origami Shapes with Cadnano. *Nucleic Acids Res.* **2009,** *37*, 5001-5006.

50. Rothemund, P., Folding DNA to Create Nanoscale Shapes and Patterns. *Nature* **2006,** *440*, 297-302.

51. Shaw, A.; Benson, E.; Högberg, B., Purification of Functionalized DNA Origami Nanostructures. *ACS Nano* **2015,** *9*, 4968-4975.

52. Camunas-Soler, J.; Ribezzi-Crivellari, M.; Ritort, F., Elastic Properties of Nucleic Acids by Single-Molecule Force Spectroscopy. *Annual Review of Biophysics* **2016,** *45*, 65-84.

53. Zheng, T. Y.; Bott, S.; Huo, Q., Techniques for Accurate Sizing of Gold Nanoparticles Using Dynamic Light Scattering with Particular Application to Chemical and Biological Sensing Based on Aggregate Formation. *ACS Appl Mater Inter* **2016,** *8*, 21585-21594.

54. Leatherdale, C. A.; Bawendi, M. G., Observation of Solvatochromism in Cdse Colloidal Quantum Dots. *Physical Review B* **2001,** *63*.

55. Debruyne, D.; Deschaume, O.; Coutino-Gonzalez, E.; Locquet, J. P.; Hofkens, J.; Van Bael, M. J.; Bartic, C., The Ph-Dependent Photoluminescence of Colloidal Cdse/Zns Quantum Dots with Different Organic Coatings. *Nanotechnology* **2015,** *26*.

56. Wolcott, A.; Doyeux, V.; Nelson, C. A.; Gearba, R.; Lei, K. W.; Yager, K. G.; Dolocan, A. D.; Williams, K.; Nguyen, D.; Zhu, X. Y., Anomalously Large Polarization Effect Responsible for Excitonic Red Shifts in Pbse Quantum Dot Solids. *J Phys Chem Lett* **2011,** *2*, 795-800.

57. Levitus, M., Tutorial: Measurement of Fluorescence Spectra and Determination of Relative Fluorescence Quantum Yields of Transparent Samples. *Methods and Applications in Fluorescence* **2020,** *8*, 033001.

58. Pal, S.; Deng, Z.; Ding, B.; Yan, H.; Liu, Y., DNA-Origami-Directed Self-Assembly of Discrete Silver-Nanoparticle Architectures. *Angew. Chem. Int. Ed.* **2010,** *49*, 2700-2704.

59. Julin, S.; Nummelin, S.; Kostiainen, M. A.; Linko, V., DNA Nanostructure-Directed Assembly of Metal Nanoparticle Superlattices. *J. Nanopart. Res.* **2018,** *20*, 119.

60. Zhu, C.; Wang, M.; Dong, J.; Zhou, C.; Wang, Q., Modular Assembly of Plasmonic Nanoparticles Assisted by DNA Origami. *Langmuir* **2018,** *34*, 14963-14968.

61. Ko, S. H.; Gallatin, G. M.; Liddle, J. A., Nanomanufacturing with DNA Origami: Factors Affecting the Kinetics and Yield of Quantum Dot Binding. *Adv. Funct. Mater.* **2012,** *22*, 1015-1023.

62. Wang, R.; Nuckolls, C.; Wind, S. J., Assembly of Heterogeneous Functional Nanomaterials on DNA Origami Scaffolds. *Angew. Chem. Int. Ed.* **2012,** *51*, 11325-11327.

63. Sharma, J.; Ke, Y.; Lin, C.; Chhabra, R.; Wang, Q.; Nangreave, J.; Liu, Y.; Yan, H., DNA-Tile-Directed Self-Assembly of Quantum Dots into Two-Dimensional Nanopatterns. *Angew. Chem. Int. Ed.* **2008,** *47*, 5157-5159.

64. Lakowicz, J. R., *Principles of Fluorescence Spectroscopy*. 3 ed.; Springer New York, NY: 2006; p 954.

65. Li, F.; Zhang, H.; Dever, B.; Li, X.-F.; Le, X. C., Thermal Stability of DNA Functionalized Gold Nanoparticles. *Bioconjugate Chemistry* **2013,** *24*, 1790-1797.

66. Li, Y.; Shen, B.; Liu, L.; Xu, H.; Zhong, X., Stable Water-Soluble Quantum Dots Capped by Poly(Ethylene Glycol) Modified Dithiocarbamate. *Colloids Surf. Physicochem. Eng. Aspects* **2012,** *410*, 144-152.

67. Hildebrandt, N.; Spillmann, C. M.; Algar, W. R.; Pons, T.; Stewart, M. H.; Oh, E.; Susumu, K.; Díaz, S. A.; Delehanty, J. B.; Medintz, I. L., Energy Transfer with Semiconductor Quantum Dot Bioconjugates: A Versatile Platform for Biosensing, Energy Harvesting, and Other Developing Applications. *Chem. Rev.* **2017,** *117*, 536-711.

TOC